Numerical study of self-camber for timber and timber-concrete composite elements by swelling hardwood inlays

Author(s):
Grönquist, Philippe (ID); Müller, Katharina; Imfeld, Luca; Frangi, Andrea (ID)

NUMERICAL STUDY OF SELF-CAMBER FOR TIMBER AND TIMBER-CONCRETE COMPOSITE ELEMENTS BY SWELLING HARDWOOD INLAYS

Philippe Grönquist[1]*, Katharina Müller[1]*, Luca Imfeld[1]*, Andrea Frangi[1]

ABSTRACT: The often-decisive criterion for the design of timber-concrete composite (TCC) slabs is the limitation of the deflections. Especially, initial deflections of the timber part occurring during the construction state due to the added weight of fresh concrete are highly contributing to total long-term deflections. Existing measures to limit the initial deflections hinder the construction process, are time consuming, or can impair the wooden elements. Self-camber by swelling hardwood inlays, a concept to level out deflections for TCC slabs, can be used. The timber elements are programmed to camber without external force influence by solely inserting dry inlays, that expand by taking up moisture, into cuts in the upper side of the timber. This paper discusses the concept of self-camber as analysed by a parametric Finite Element study of inlay configuration. We show that the required target camber for compensating the deflections can be reached and provide guidelines to design the inlay configuration.

KEYWORDS: parametric modelling, pre-camber, self-camber, self-shaping, swelling inlay, timber-concrete composite slab

1 INTRODUCTION

A way of effectively addressing the increasing demand for sustainable construction materials is to consider the materialization and building technology of floor slabs. Floor slabs account by far for the largest share of volume in any building and have so far largely been made of reinforced concrete. Nowadays, slabs can also be made from high-performance timber products such as dowel-laminated timber, cross-laminated timber, or TCC elements [1]. These types of slabs offer a more climate-friendly alternative to pure reinforced concrete [2]. However, a common and prevalent design problem of timber and TCC slabs are the high deflections that need to fulfill a given serviceability limit state (SLS) enforced by structural design guidelines [3]. Along with vibration limitation, the deflection limitation is usually the main design criteria. Therefore, lowering the deflections can reduce and optimize the usage of both concrete and timber.

For on-site produced TCC slabs, the main deflections are caused during the construction by the self-weight of the fresh concrete or the floor screed poured on top of the timber elements. These high initial deflections significantly contribute to the total long-term deflections relevant for the design of the SLS [4,5]. Therefore, their minimization is of high interest. Conventionally, this can entail a huge impact on time and costs of the construction. In fact, there are several existing measures against the initial deflections during the construction: The timber elements can be propped during the casting of the concrete, where the propping needs to stay in place until the concrete has hardened. Propping is therefore material and time consuming and interferes with the construction site. Another option is the cambering of the timber elements by mechanical bending of every slat or cutting the element into a bent shape during the timber prefabrication. Both options are costly, and cut fibers weaken the load-carrying capacity of the timber. Prefabrication of the TCC slab in form of pouring and hardening of the concrete in a factory is the least laborious measure. However, prefabricated elements can complicate the transport, and in some cases, on-site concreting is the only available option.

This paper investigates a method to camber timber elements in a short time, on site, and without external forces. Swelling hardwood inlays, inserted in an oven-dry state into pre-cut notches in the softwood timber beams will exert a swelling pressure onto the notches while taking up moisture from the environment. The expansion forces, i.e. the swelling pressure resultants, and their eccentricity to the longitudinal axis induce a negative moment on the beam. This results in a self-cambering of the beam (denoted as $w(c)$, see illustration in Figure 1). The self-weight of fresh concrete or screed poured on top will result in deflections $w(q)$. Therefore, a target value of the self-camber can be represented as $w(c) = -w(q)$.

Using wood's inherent hygroscopic capacity for generating residual strain or stress by moisture changes in response to humidity changes is a known solution and has been used previously, e.g. in timber structures manufacturing in the context of producing curved components by self-shaping [6,7]. The concept of

swelling hardwood inlays in timber beams for internal force generation and self-shaping has also been investigated previously using densified wood [8,9]. However, studies showed that native European beech wood comparatively reaches sufficient swelling pressure by restrained swelling [10]. Therefore, the use of the more expensive option of densified wood is not necessary.
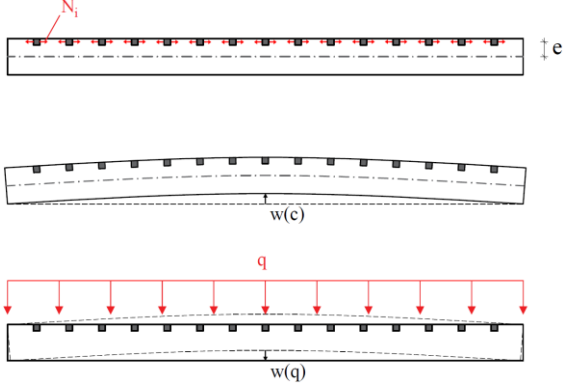

Figure 1: Concept of self-camber by expanding inlays. Normal force N_i generated by swelling pressure of inlays leads to upwards deflection $w(c)$ due to eccentricity e. After addition of concrete (load q, concrete weight), deflection is optimally compensated such that $w(c) + w(q) = 0$.

In this study, European beech (*Fagus sylvatica L.*) was chosen as the theoretical inlay material. This species of hardwood displays both a high transversal stiffness and swelling coefficient as compared to other European native species. Therefore, it is well suited for developing the necessary swelling pressure to induce the self-camber. The timber component of the analyzed slab section was chosen to be dowel-laminated timber (also referred to as Brettstapel). In order to analyze the amount of self-camber resulting from a given swelling inlay configuration in a parametric manner, a numerical Finite Element (FE) model was used. Different aspects such as geometry and orientation of the inlays, or span of the beam were analyzed. The target camber of the respective con-figurations was calculated for different spans using sections of TCC slabs that fulfill design rules according to structural standards. Based on the results, design possibilities for the self-cambering of TCC elements using swelling hardwood inlays are discussed.

2 METHODS

2.1 NUMERICAL MODEL

A numerical and parametric simulation model was developed for a 3D FE static analysis within the commercial software *Abaqus 6.14*. The assembly of the model follows the assembly of a unit beam of a dowel-laminated timber slab being composed of timber boards (Norway spruce, *Picea abies*) connected by cylindrical hardwood dowels (European beech, *Fagus sylvatica L*) with a diameter of 20 mm, including notches for the swelling beech wood inlays (see Figure 2a). The unit beam was modelled as simply supported system loaded only by its self-weight. The beam and dowels were connected by *tie*-constraints, and the beam and inlays were connected by *surface to surface* contact conditions (*hard contact*, assumption of tangential friction coefficient of 0.4 for wood on wood in dry condition). The elements for all parts were chosen as 20-node quadratic elements with reduced integration (*C3D20R*). The beech wood inlays were subjected to a steady-state wood moisture content (MC) change of 12%, swelling from an oven-dry state (0% MC) to an equilibrium state at approximately 65% relative humidity at 20°C (12% MC). The spruce beam was kept at a constant moisture level of 12% MC throughout the analysis.

The beech and spruce wood components were modelled using a 3D orthotropic linear elastic material law in order to account for the three wood anatomical directions (R: Radial, T: Tangential, L: Longitudinal). Hereby, the following material compliance matrix was used in order to relate the total stress tensors and the elastic strain tensors ($\boldsymbol{\varepsilon}_{el} = \boldsymbol{C}^{-1} : \boldsymbol{\sigma}$):

$$\boldsymbol{C}^{-1} = \begin{bmatrix} \dfrac{1}{E_R} & \dfrac{-\nu_{TR}}{E_T} & \dfrac{-\nu_{LR}}{E_L} & 0 & 0 & 0 \\[2mm] \dfrac{-\nu_{RT}}{E_R} & \dfrac{1}{E_T} & \dfrac{-\nu_{LT}}{E_L} & 0 & 0 & 0 \\[2mm] \dfrac{-\nu_{RL}}{E_R} & \dfrac{-\nu_{TL}}{E_T} & \dfrac{1}{E_L} & 0 & 0 & 0 \\[2mm] 0 & 0 & 0 & \dfrac{1}{G_{RT}} & 0 & 0 \\[2mm] 0 & 0 & 0 & 0 & \dfrac{1}{G_{RL}} & 0 \\[2mm] 0 & 0 & 0 & 0 & 0 & \dfrac{1}{G_{TL}} \end{bmatrix}. \quad (1)$$

All nine independent engineering constants P_b (for beech wood) and P_s (for spruce wood) of $\boldsymbol{C}^{-1}$ were calculated as function of the actual MC, denoted ω, as:

Table 1: Coefficients for determination of moisture dependent elastic properties $\boldsymbol{P_b}$ and $\boldsymbol{P_s}$ (equations (2) and (3)) of beech and spruce wood (from [11]).

	E_R (MPa)	E_T (MPa)	E_L (MPa)	G_{RT} (MPa)	G_{RL} (MPa)	G_{TL} (MPa)	ν_{TR} (x10^{-3})	ν_{LR} (x10^{-3})	ν_{LT} (x10^{-3})
b_0	2565.6	885.4	17136.7	667.8	1482	1100	293.3	383.0	336.8
b_1	-59.7	-23.4	-282.4	-15.19	-15.26	-17.72	-1.012	-8.722	-9.071
s_0	999.64	506.08	12791.75	61.33	762.8	880.75	153.4	232.0	285.7
s_1	3.61	5.0	15.22	-1.07	5.93	1.39	10.8	-8.6	-41.0
s_2	-2.09	-1.35	-9.01	-0.06	-1.99	-1.39	0.398	2.878	7.191
s_3	0.0467	0.0297	0.1885	0.0017	0.0477	0.0277	-0.0191	-0.0786	-0.1642

$$P_b = b_0 + b_1\omega \qquad (2)$$

$$P_s = s_0 + s_1\omega + s_2\omega^2 + s_3\omega^3. \qquad (3)$$

The values of the parameters b_i and s_i, taken from Hassani et al. [11], are shown in Table 1 above.

In the model, the stresses driving the self-cambering result purely from hindered swelling. The swelling strain $\boldsymbol{\varepsilon}_{sw} = \boldsymbol{\alpha}\Delta\omega$ was modelled using the differential moisture expansion coefficients (elements of diagonal coefficient tensor $\boldsymbol{\alpha}$) shown in Table 2. As small deformations were assumed, the total strain tensor during the analysis was chosen to be a superposition of the elastic strains and the swelling strains: $\boldsymbol{\varepsilon}_{tot} = \boldsymbol{\varepsilon}_{el} + \boldsymbol{\varepsilon}_{sw}$ (subscripts "el" for elasticity and "sw" for swelling). Hereby, $\boldsymbol{\varepsilon}_{sw}$ does not contribute to the free energy function during the analysis, i.e., volume changes do not affect total energy. However, strain energy is created when the swelling is restrained.

Table 2: *Differential swelling coefficients in R, T, and L anatomical directions for European beech wood (from* [11]*).*

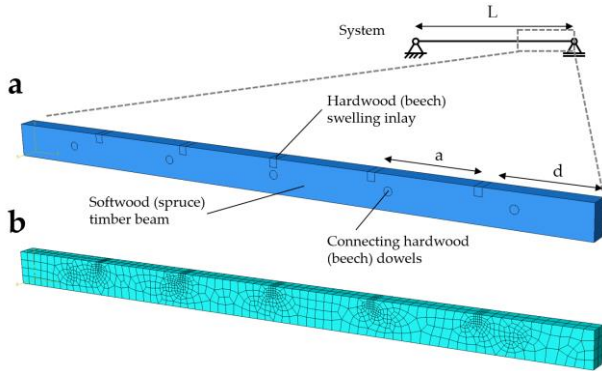| α_R (1/%)	α_T (1/%)	α_L (1/%)
0.00191	0.00462	0.00011

Figure 2: a: *Assembly of exemplary system of numerical model composed by three components (beam, inlays, and dowels). Local coordinate systems of components are shown in Figure 3a.* **b:** *Visualization of used mesh for FE analysis.*

2.2 PARAMETRIC ANALYSIS PROCEDURE

A multi-step approach procedure was chosen in order to cover a wide parametric space of possible designs of inlay configuration. First, the self-camber was analyzed in dependence of the inlay orientation. The inlays can be placed tangentially or radially oriented (Figure 3b). In a next step, different possible shapes of inlays were analyzed, namely rectangular, semi-octagonal, semi-rounded, and a wedge-type of shape (Figure 3c). Subsequently, different geometries, varying width and height of the inlays, were analyzed. All the analyses were conducted by simultaneously varying distancing and number of inlays, keeping a fixed beam span of 4 m. Using optimized configuration designs from the previous steps, calculations were also conducted for two further and practically more relevant spans of 6 m and 8 m. Finally, the simple and quick linear elastic modelling approach was verified for a given design space (square inlays, 4 m span) by conducting computation-heavy model analyses using a complex rheological model for wood, described by Hassani et al. [11]. Hereby, visco-

elasticity of the wood components is modelled by a series of four Kelvin-Voigt rheological elements for both spruce and beech wood, while mechanosorption is modelled as a series of three of such elements. Plasticity is modelled by a multi-surface yield criterion with a Ramberg-Osgood type hardening. For the latter analysis, the total strain tensor decomposes as $\boldsymbol{\varepsilon}_{tot} = \boldsymbol{\varepsilon}_{el} + \boldsymbol{\varepsilon}_{sw} + \boldsymbol{\varepsilon}_{ve} + \boldsymbol{\varepsilon}_{ms} + \boldsymbol{\varepsilon}_{pl}$ (subscripts "ve" for viscoelasticity, "ms" for mechanosorption, and "pl" for plasticity). Complete model details and parameters can be found in [11].
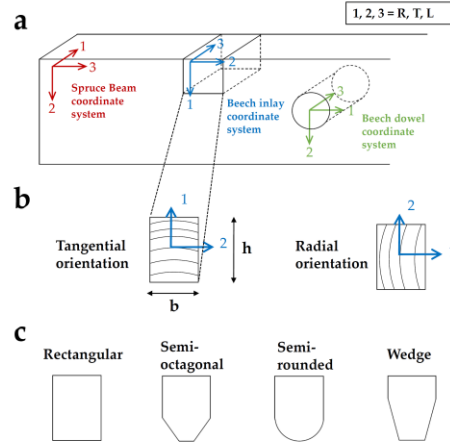

Figure 3: a: *Single model components (beam, inlays, dowels) with their local coordinate systems 1,2,3 corresponding to wood anatomical directions R,T,L.* **b:** *Tangential versus radial orientation of inlays (height h and width b).* **c:** *Different analyzed shapes of inlays.*

2.3 BOUNDARIES

The distance of inlays (a) and the distance of inlays to the edge (d) of the beam (see Figure 2a) are parametric values with limitations set by design standards (e.g. [12]). The primary limitation serves to avoid shear failure in the beam at the notches close to the edges (possible failures in LT or LR planes). Hereby the following criterion was used to limit the parametric analysis:

$$d_{min} \geq \frac{\sigma_{sw} \cdot h}{f_{v,k}} \qquad (4)$$

The minimal distance d_{min} of the notches to the edge depends on the height h of the notches, the characteristic value of the shear strength $f_{v,k}$ of the spruce board ($f_{v,k} = 4.0$ N/mm^2), and on the elastic swelling pressure $\sigma_{sw} = \alpha_T\Delta\omega E_{c,90,mean}$ (α_T: transversal swelling coefficient of beech inlay, $\Delta\omega$: Wood moisture content change, $E_{c,90,mean} = 300$ N/mm^2: Mean value of transversal elastic stiffness of beech inlay). This theoretical value of the swelling pressure will result in a highly conservative criterion.

Further parametric limitations include a non-overlap condition of the notches to neighboring as well as a non-overlap condition of dowels to notches. The distance a between inlays is resulting from the following relation:

$$a = \frac{L - 2d - nb}{n - 1}, \qquad (5)$$

where L is the span of the beam, n is the number of inlays, and b is the width of inlays. Finally, the geometric boundary conditions of the beam and the dowels were chosen as shown in Table 3. These, including the height of the concrete for the calculation of target camber, remain constant throughout the analyses regardless of inlay parametrization.

Table 3: Geometric boundary conditions of parametric analysis in dependence of: L: beam span, h_b: height of spruce beam, $h_{b,red}$: reduced beam height due to the notches, h_c: height of concrete (values according to typical TCC slab design), and n_d: number of connection dowels between spruce beams.

L (m)	h_b (mm)	$h_{b,red}$ (mm)	h_c (mm)	n_d
4.0	120	85	70	13
6.0	130	90	70	15
8.0	170	115	110	25

2.4 TARGET CAMBER

The target value for the self-camber to compensate the deflections can be defined according to different requirements: (I) short-term, elastic deflections of the timber element caused by the self-weight of fresh concrete during the construction; (II) short-term, elastic deflections of the timber or composite slab caused by self-weight and dead load (floor construction); and (III) long-term deflections of the timber or composite slab caused by self-weight, dead load and permanent value of the live load. These deflections can be calculated for each case of desired slab system according to EC-1995-1-1 [3] and further state of the art and research [4]. In the present numerical study, the aim is to compensate the deflections in state (I), such as to eliminate the need of propping during construction and to result in an initially fully flat slab (no curvature of the beam during hardening of the concrete). The target camber w(q) was therefore calculated for the simply supported beams with

$$w(q) = \frac{5}{384} \frac{(g_{k,t} + g_{k,c} + q_{k,C})L^4}{E_{t,0}I_{y,t}}. \tag{6}$$

The variables $g_{k,t}$, $g_{k,c}$, $q_{k,C}$ represent the dead load of timber, the dead load of concrete, and the possible temporary live load during construction. $E_{t,0} = 11'000$ N/mm^2 is the assumed mean value of the elastic modulus of the spruce timber beam, and $I_{y,t} = h_{b,red}^3/12$ is the area moment of inertia of the beam per unit width (conservative calculation). Table 4 summarizes the used values and results obtained.

Table 4: Load values used to calculate target camber w(q) in dependence of span. Dead loads $g_{k,t}$ follow values according to boundary conditions (see Table 3, $g_{k,t} = \rho_{k,t}gh_b$ and $g_{k,c} = \gamma_c h_c$ with $g = 9.81$ m/s^2, $\rho_{k,t} = 500$ kg/m^3 and $\gamma_c = 25$ kN/m^3).

L (m)	$g_{k,t}$ (kN/m^2)	$g_{k,c}$ (kN/m^2)	$q_{k,C}$ (kN/m^2)	w(q) (mm)
4.0	0.60	1.75	1.0	19.8
6.0	0.65	1.75	1.0	85.9
8.0	0.85	2.75	1.0	176.0

3 RESULTS AND DISCUSSION

3.1 INLAY ORIENTATION

Figure 4 shows the amount of self-camber in dependence of inlay orientation for the case of a beam of 4 m span with different number of square inlays (n = 8, 15, 26) and with different spacing of the inlays a. It can be recognized that in all models the largest amount of self-camber is realized by tangentially oriented inlays. This is valid regardless of the number of inlays or the spacing. An exception is the extreme case of n = 26 and a = 25 mm, where w(c) is equal for both orientations. In general, more inlays and less spacing tend to result in higher self-camber. However, inlays too closely spaced diminish w(c) in the case of n = 8 and n = 15 for tangentially oriented inlays.
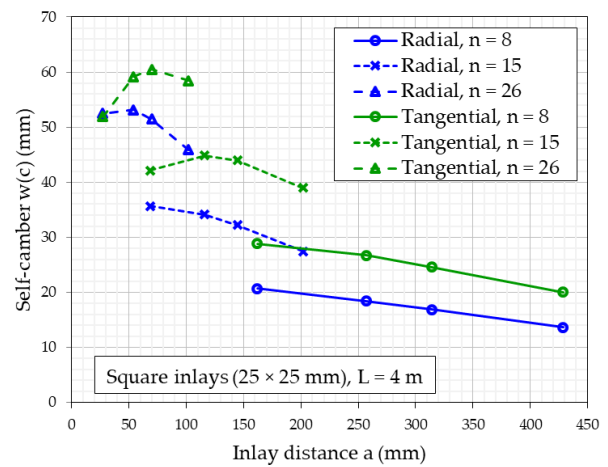

Figure 4: Self-camber of a 4 m long and simply supported beam in function of orientation (radial or tangential), number of swelling inlays (n), and inlay distance. Inlays are square with dimensions 25x25 mm.

The larger self-camber of tangential inlays can be explained by the fact that the tangential swelling coefficient of beech wood is nearly double the value of the radial one (see Table 2). On the other hand, the radial stiffness of beech is more than double of the tangential stiffness (see Table 1). Since the resulting swelling pressure (hindered swelling) is both dependent on stiffness and expansion coefficient of the swelling material, both radially and tangentially oriented inlays are expected to result in comparable camber values. However, in the case of a pure elastic embedding (here, beech inlays against spruce beam), the influence of stiffness of the swelling material is reduced in comparison to influence of swelling coefficient. This can explain the higher elastic self-camber of tangential inlays.

For the subsequent steps of the parametric study, a tangential orientation was chosen for all the models. However, it should be noted that these results are valid only for a pure linear-elastic calculation. In reality, the material law for transversal beech wood can be represented by Ramberg-Osgood curves [13]. Therefore, and based on the data shown in [10,13], it should be noted that radially oriented inlays in reality will reach higher swelling pressures for high differences in MC.

3.2 SHAPE OF INLAYS

Figure 5 shows the self-camber w(c) in dependence of the four different inlay shapes rectangular, semi-octagonal, semi-round, and wedge-type. The span is fixed to 4 m and the height and width of the inlays to 30 mm and 25 mm. The results show that the rectangular shape achieves a clearly higher self-camber than the other shapes. For all the other shapes, the values for self-camber are comparable. This observation can be made regardless of the number of inlays and the inlay spacing. Therefore, even though the other inlay shapes would result in a smoother shear stress transfer (no sharp notches in the spruce beam and thus no shear stress peaks), the rectangular shape results in a higher swelling pressure resultant because of the higher volume of swelling material. Next to achieving higher w(c), a rectangular shape is also beneficial in terms of fabrication and machining of both notched beam and inlays. Therefore, square or rectangular shapes are preferred over other shapes.
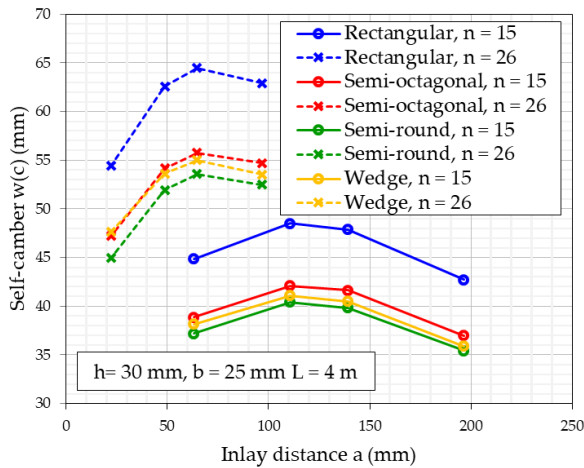

Figure 5: Self-camber of a 4 m long and simply supported beam in function of the number (n) of inlays, the shape of inlays (4 different shapes), and the inlay distance. Inlays possess height (h) of 30 mm and width (b) of 25 mm.

3.3 INLAY GEOMETRY

Figure 6 shows the self-camber w(c) as function of the distance a, the inlay number n, and the inlay height h, where h was varied from 25 to 30 mm, while the width b was kept constant at 25 mm. It can be seen that, similar as in the previous Figures 4 and 5 (same span of 4 m), a higher inlay number n and a lower distance a tend to result in a larger w(c). In all the configurations, a higher inlay height resulted in a higher w(c). In comparison to Figure 7, where a fixed height of 25 mm was maintained but the width was varied between 25 and 35 mm, it can be seen that varying the height (at constant width) has an overall larger influence on w(c) than varying width (at constant height). This result may at first appear counter-intuitive because a larger height of inlay automatically entails a lower eccentricity of the swelling pressure resultant with respect to the central axis of the beam. However, this effect can be attributed to the deeper notches that highly reduce the area moment of inertia $I_{y,t}$,

which results in a higher self-camber. Varying the width of the notches has no influence on the latter. Therefore, it can be noted that not only swelling pressure is important in dictating the magnitude of w(c), but also the bending stiffness of the notched beam. In terms of achieving larger swelling pressure only, varying b would appear more impactful as the restrained swelling length is directly affected. As a conclusion, if a larger amount of w(c) is desired, e.g. where the span of the beam increases, it is more economic varying the height of the inlays rather than their width.
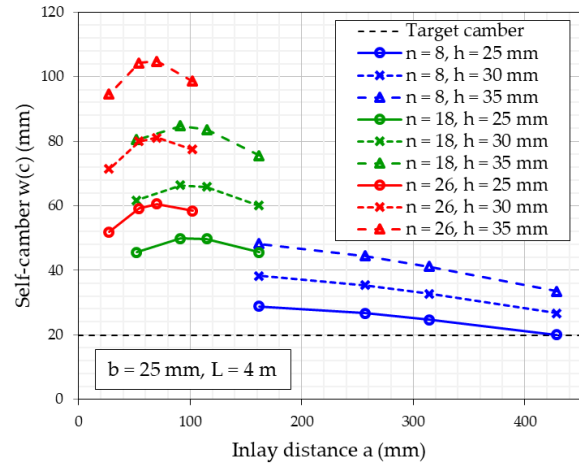

Figure 6: Self-camber of a 4 m long and simply supported beam in function of the number (n) of inlays, the height (h) of inlays, and the inlay distance. Inlays are rectangular with fixed width (b) of 25 mm.
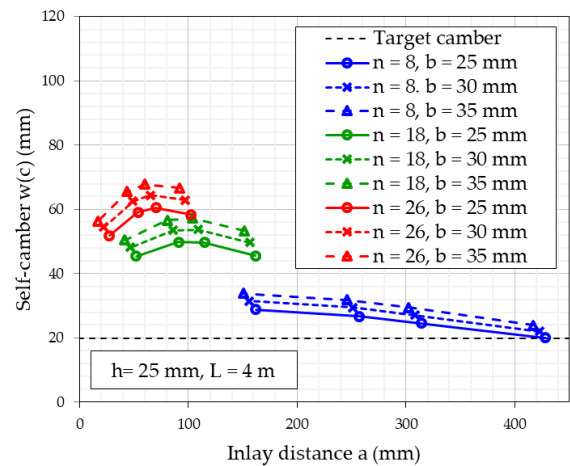

Figure 7: Self-camber of a 4 m long and simply supported beam in function of the number (n) of inlays, the width (b) of inlays, and the inlay distance. Inlays are rectangular with fixed height (h) of 25 mm.

3.4 INFLUENCE OF SPAN

In the previous analyses, the span was fixed to a constant value of 4 m. However, since the required self-camber is largely a function of the span of the beam, and since 4 m still represents a low span according to nowadays requirements for slabs, e.g. in multi-story office buildings, spans of 6 and 8 m were also analyzed. Figures 8 and 9 show w(c) for spans of 6 and 8 m respectively, in function

of a, n, and h, and for rectangular inlays with fixed widths $b = 30$ mm and $b = 35$ mm. As in the previous analyses, a larger number of inlays and a larger height of inlays reach higher self-camber.
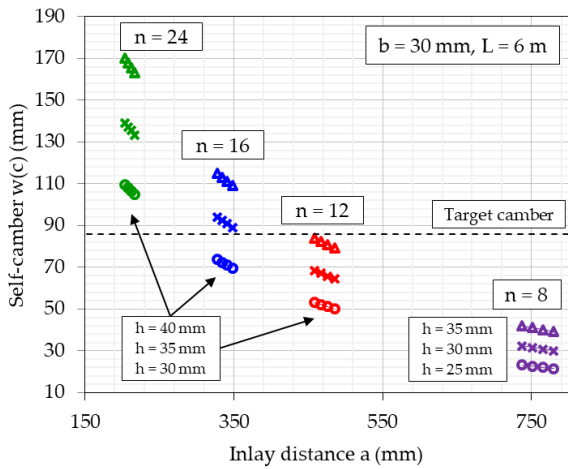

Figure 8: Self-camber of a 6 m long and simply supported beam in function of the number (n, separated by colors) of inlays, the height (h, separated by symbols) of inlays, and the inlay distance. Inlays are rectangular with fixed width (b) of 30 mm.
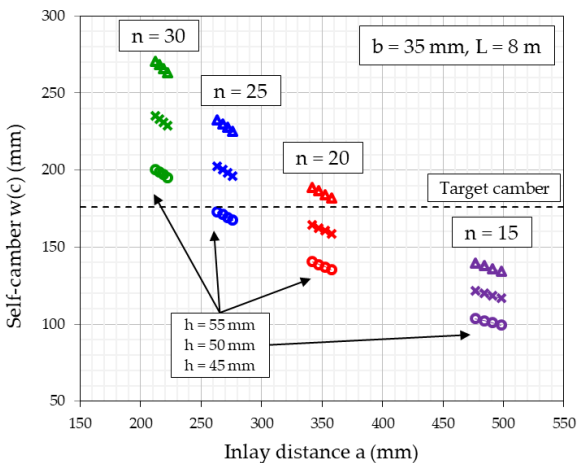

Figure 9: Self-camber of a 8 m long and simply supported beam in function of the number (n, separated by colors) of inlays, the height (h, separated by symbols) of inlays, and the inlay distance. Inlays are rectangular with fixed width (b) of 35 mm.

It can be seen that the target camber appears to be more difficult to reach with similar configurations for spans of 6 and 8 meters than for a shorter span of 4 meters (see Figures 6-9). This can be explained by the fact that w(q) is increasing with the power of four of the span while the self-camber w(c) is not dependent on the span length. Therefore, larger spans require a disproportionally higher number of inlays and result in intensive machining. Self-camber by swelling inlays is thus more efficient and less costly for smaller spans. However, it should be noted that by increasing the span, the height of the beam is automatically also increased (see Table 3) in order to fulfill the structural requirements of the planned TCC slab. Therefore, it is difficult to compare different spans with respect to parametric influence on w(c). Still, Figures

8 and 9 allow for the conclusion that for each span an optimal configuration of inlays exists with respect to reaching target camber. Generally, the larger the span, the larger the number and height of required inlays to compensate w(q).

3.5 ANALYSIS USING A RHEOLOGICAL MATERIAL LAW

Next to the complete set of geometrical parameters investigated above, the material law used in the analysis has a decisive impact. E.g., it is known that wood creeps under sustained stress (entailing a stress relaxation in case of residual stresses) and that it can be deformed irreversibly under high compression stress (plasticity). Both of these mechanisms are influenced by time, amount of moisture change, and moisture level. Especially for self-camber induced by residual swelling stress, such effects are non-negligible, as can be demonstrated by the results shown in Figure 10. The comparison to the linear-elastic-only material law is made using a span of 4 m with 26 square inlays, and for different distancing of the inlays.
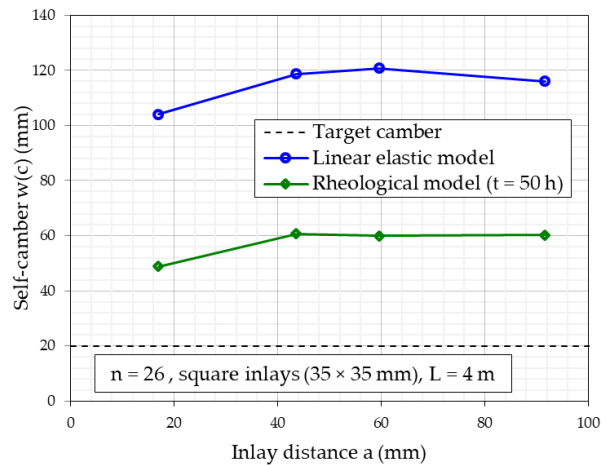

Figure 10: Self-camber of a 4 m long and simply supported beam with 26 inlays in function of the constitutive material model used for simulation and the inlay distance. Inlays are square with dimensions 35 x 35 mm.

The achieved self-camber using a complex rheological model is nearly half the value of the model using a linear-elastic material law only. This means that the effective swelling pressure resultant has a lower value, and that in reality w(c) is expected to reach lower values than what is shown in the previous Figures. However, Figure 10 also shows that the qualitative parametric behavior is similar, which validates using a linear-elastic material law for the simplified and computationally-light parametric analyses conducted above. It is also shown that the target camber is reached with both material models for this particular system.

3.6 DESIGN OF SELF-CAMBER OF TCC ELEMENTS

In summary, the conducted parametric analysis has led to the following conclusions such that the self-cambering can be maximized:

- A tangential orientation of inlays is preferred over a radial orientation if the change in MC is low. For high changes in MC, it is the other way around.
- A rectangular shape of inlays is preferred over other more complex shapes.
- In order to increase w(c) for rectangular inlays, increasing inlay height is preferred over increasing width.
- Generally, w(c) increases with more inlays and with lower spacing of inlays.
- Different spans are not directly comparable because of their different cross-sections. However, w(q) increases proportionally to L^4 and w(c) does not. Therefore, in the context of TCC slabs, the concept and effort of self-camber is more economical for smaller spans.
- Self-camber as calculated by linear elastic models is expected to be largely reduced due to stress-relaxation effects of the wood. Therefore, the results shown in this study are of qualitative nature only.

Further combined experimental and numerical studies still need to be conducted in order to address the latter issue. E.g. in order to assess effects such as scale influences in wood and their effect [14]. An example could be the local influence of knots in the dowelled-laminated timber boards, which were omitted in this study.

Regarding the design, i.e. deciding on both the target camber and on inlay configuration, the following considerations are relevant:

- The target camber should be chosen so that the concrete is able to harden in a nearly flat state in order to avoid a notable discontinuous thickness over the length of the TCC slab. For this reason, only a compensation of deflections caused by the wet concrete weight might be desirable.
- The results showed that an inlay configuration can be found for every situation, such that w(c) = - w(q) can be fulfilled, even by theoretical reduction due to creep effects. However, it should be noted that this equality may be critical in some situations (like above), and that for this reason, the models to predict both w(c) and w(q) need to be as precise as possible.
- Assuming a perfect prediction model in terms of material and geometry, w(c) is fixed for a given inlay configuration only for a predefined and specific change in MC. In fact, the difference in MC can always be adapted and is a decisive parameter as well, as w(c) is directly proportional to $\Delta\omega$. In any experimental assessment, it is therefore crucial to monitor the MC. In practical situations, the MC may even be used to adjust w(c) to a desired value by controlling the climate (relative humidity and temperature).
- The swelling time, or time taken from insertion to reaching full swelling pressure generation is dependent on $\Delta\omega$, which is in turn dependent on moisture diffusion processes and boundary conditions. However, the small dimensions of the inlays would allow for a fast moisture diffusion process that enables low waiting times in between inlay insertion and on-site pouring possibility of the concrete. In addition, in the case of high MC differences (e.g. $\Delta\omega = 12\%$), maximal swelling pressure will be reached before moisture diffusion is complete due to reaching yield stress of the inlay before.

This conceptual preliminary study was restricted to analysis of inlay configuration and did not include assessment on the important aspect of the connection between timber and concrete. In the case of TCC with dowel-laminated timber, multiple efficient and compatible solutions for connection systems are deemed possible, e.g. a connection by micro-notches [15,16]. The notches for the inlays may even be directly used as shear connectors for the concrete.

4 CONCLUSIONS

The investigations using a parametric numerical model gave valuable insight on the feasibility and opportunities of self-cambering timber elements by swelling hardwood inlays. This principle could allow for future more economic dimensioning of TCC cross-sections by efficiently compensating initial deflections in the case of on-site produced TCC slabs. Even though it was found that the values of self-camber obtained in the linear-elastic numerical simulations were not accountable in a quantitative manner, a given target-camber can always be compensated. In addition, the inlay configuration-dependent behaviour is expected to be qualitatively similar to the results shown.

REFERENCES

[1] D. Yeoh, M. Fragiacomo, M. De Franceschi, and K. H. Boon, "State of the Art on Timber-Concrete Composite Structures: Literature Review," *J. Struct. Eng.*, vol. 137, no. 10, pp. 1085–1095, 2011.

[2] A. M. P. G. Dias, J. Skinner, K. Crews, and T. Tannert, "Timber-concrete-composites increasing the use of timber in construction," *Eur. J. Wood Wood Prod.*, vol. 74, no. 3, pp. 443–451, 2016.

[3] CEN European Committee for Standardization, "Eurocode 5 : Design of timber structures - Part 1-1 : General - Common rules and rules for buildings," *Design*. pp. 1–123, 2004.

[4] A. M. P. G. Dias, J. Schänzlin, and P. Dietsch, *Design of timber-concrete composite structures: A state-of-the-art report by COST Action FP1402 / WG 4*. 2018.

[5]   M. Fragiacomo and E. Lukaszewska, "Influence of the Construction Method on the Long-Term Behavior of Timber-Concrete Composite Beams," *J. Struct. Eng.*, vol. 141, no. 10, p. 04015013, 2015.

[6]   P. Grönquist, D. Wood, M. M. Hassani, F. K. Wittel, A. Menges, and M. Rüggeberg, "Analysis of hygroscopic self-shaping wood at large scale for curved mass timber structures," *Sci. Adv.*, vol. 5, no. 9, 2019.

[7]   D. Wood *et al.*, "From machine control to material programming:," in *Fabricate 2020*, UCL Press, 2020, pp. 50–57.

[8]   B. Anshari and Z. W. Guan, "Numerical Modelling of the Initial Stress and Upward Deflection of Glulam Beams Pre-Stresseed by Compressed Wood," *Appl. Mech. Mater.*, vol. 493, pp. 408–413, 2014.

[9]   B. Anshari, Z. W. Guan, and Q. Y. Wang, "Modelling of Glulam beams pre-stressed by compressed wood," *Compos. Struct.*, vol. 165, pp. 160–170, Apr. 2017.

[10]   P. Grönquist *et al.*, "Investigations on densified beech wood for application as a swelling dowel in timber joints," *Holzforschung*, vol. 73, no. 6, 2019.

[11]   M. M. Hassani, F. K. Wittel, S. Hering, and H. J. Herrmann, "Rheological model for wood," *Comput. Methods Appl. Mech. Eng.*, vol. 283, pp. 1032–1060, 2015.

[12]   SIA Swiss Society of Engineers and Architects, "SIA 265: Holzbau." 2012.

[13]   Hering, S., Saft, S., Resch, E., Niemz, P., & Kaliske, M.   "Characterisation of moisture-dependent plasticity of beech wood and its application to a multi-surface plasticity model", *Holzforschung*, vol. 66, no. 3, pp. 373-380, 2012.

[14]   J. Füssl, M. Lukacevic, S. Pillwein, and H. Pottmann, "Computational mechanical modelling of wood—from microstructural characteristics over wood-based products to advanced timber structures," in *Lecture Notes in Civil Engineering*, vol. 24, Springer, 2019, pp. 639–673.

[15]   K. Müller and A. Frangi, "4-Point Bending Tests of Timber-Concrete Composite Slabs with Micro-Notches," in *WCTE 2018 - World Conference on Timber Engineering*, 2018, pp. 4–5.

[16]   K. Müller, "Timber-concrete composite slabs with micro-notches", PhD Thesis, ETH Zurich, 2020.